Korean J. Chem. Eng., **25**(1), 78-83 (2008)

Characterization of fly ash-pastes synthesized at different activator conditions

Sang-Sook Park and Hwa-Young Kang*,†

Division of Civil and Environmental Engineering, Sunchon National University, Sunchon 540-742, Korea
*Department of Civil and Environment, Hanyeong Technical College, Yeosu 550-704, Korea
(*Received 2 November 2006 • accepted 11 June 2007*)

Abstract−Compressive strength and mineralogical and microstructural characterization of the pastes prepared from alkali-activation of low calcium fly ash were investigated. XRD and FTIR were used to observe the mineralogical characterization; SEM, MIP, and NMR were used to observe the microstructural characterization of the pastes. The higher strength of paste was attributed to a more compact and continuous gelatinous matrix due to restructuring of reaction product. The lower values of both porosity (31.0%) and mean pore diameter (9.7 nm) of fly ash-pastes alkali-activated at 85 °C for 24 hr indicate higher reactivity of these pastes compared with other pastes, and result in the higher compressive strength.

Key words: Fly Ash, Alkali Activation, Microstructure, Mercury Porosimetry

INTRODUCTION

The production of Portland cement not only consumes limestone, clay, coal, and electric power, but also releases waste gases, such as CO_2, SO_3, and NO_x, which can cause the greenhouse effect and acid rain [1]. Therefore, it is a valid method to use the industrial by-products as replacement of Portland cement. One the other hand, the demand for industrial and domestic energy results in the production of a large volume of fly ash from solid coal fuel, which will increase in the world on an unprecedented scale during the coming years (800×10^6 tons by the year 2010). Only a small part of this ash is used at present (20-30%); the rest is landfilled and surface-impounded, with potential risks of air pollution, contamination of water due to leeching, etc. [2,3]. Therefore, fly ash should not only be disposed of safely to prevent environmental pollution, but should be treated as a valuable resource. As a result, the method of alkali-activation to convert fly ash into cementitious material without Portland cement has generated considerable interest.

The alkaline activators that have been used for activating fly ash include NaOH, KOH, Na_2CO_3, Na_2SO_4, and water glass solution. Recent work by Xie and Xi [4] indicates that the effect of activation strongly depends on the physical-chemical nature of the fly ash and the type of activator. Hossein and William [5] present that concrete prepared from alkali activation of class F fly ash has high ultimate strength (110 MPa), excellent acid resistance and freeze-thaw durability. It was found that this concrete is economically and technically viable for many construction applications. In previous work, Samadi [6] reports that by using class F fly ash and water glass, a high strength paste can be made with compressive strength of up to 8,000 psi after curing at 60 °C for 24 hr.

According to Arjunan et al. [7] for the alkaline activation of fly ash the OH^- attacked the surface of the fly ash particles at a high alkaline pH during the processing of the fly ash. The corroded surface provided more surface area for further attack by sodium hydroxide and, consequently, the formation of amorphous aluminosilicate was promoted [8]. Namely, alkali-activating system of fly ash requires a strongly alkaline solution to activate aluminosilicate solid dissolution [9,10]. This product is responsible for the excellent mechanical-cementitious properties of the alkali-activated fly ash. Palomo et al. [10] also indicate that the concentration of chemical species (specifically OH^-), curing temperature and time, type of alkaline element are always significative factors of the strength development of pastes of alkali-activated fly ash.

In this research work, Korean Class F fly ash was alkali-activated by a mixture composed of water glass, sodium hydroxide and water. The specific objective was to study of mineralogical and microstructural properties of the reaction product of alkali-activated fly ash pastes.

MATERIALS AND METHOD

1. Materials

Low-calcium fly ash produced from coal-fired electric power stations in Korea is used as cementitious material in this work. The chemical composition of the fly ash, as determined by analysis using a Philips PW 2404 sequential X-ray fluorescence (XRF) spectrometer, is shown in Table 1 and the chemical composition of the water glass is listed in Table 2. It should be pointed out that the fly ash used in this study has a high fraction of reactive oxides ($SiO_2+Al_2O_3+Fe_2O_3>87.41$), which means that it has high reactivity with water glass.

2. Sample Preparation

Activator/fly ash ratio of 0.6 (wt%) is selected for all samples to obtain a desirable flow of the pastes. The activator contains water glass, sodium hydroxide and water. Mixing of fly ash and activator is done by a small HJ-1150 mortar mixer at a low speed. After casting in 5×5×5 cm cubic molds, the samples are cured in sealed plastic bags in an oven of 60 °C and 85 °C for activation times. In order to verify the effectiveness of activators on strength of alkali-activated fly ash pastes, their compressive strengths are measured in the first part of the experimental program.

†To whom correspondence should be addressed.
E-mail: khy9792@hanmail.net

Table 1. Chemical composition of the raw fly ash (wt%)

Element	SiO_2	Al_2O_3	Fe_2O_3	CaO	MgO	Na_2O	K_2O	TiO_2	P_2O_5	MnO	Ig.loss
Content (%)	49.58	31.90	5.93	2.98	0.95	0.42	0.88	1.73	0.79	0.05	4.30

Table 2. Specification of water glass

Na_2O (%)	SiO_2 (%)	H_2O (%)	Na_2O/SiO_2
13.5	30.5	56.0	2.26

3. Analysis Methods

The compressive strength of all pastes is determined by KS L 5105. X-ray diffraction (XRD, Rigaku D/MAX-III B X-Ray), and a fourier transform infrared spectrometer (FTIR) is used to observe the mineralogical characterization of the pastes. Scanning electron microscopy (SEM, JEOL JSM-T330), mercury intrusion porosimetry (MIP, Micromeritics AutoPore IV 9510) and ^{29}Si and ^{27}Al NMR are used to observe the microstructural features of the pastes. The ^{29}Si and ^{27}Al NMR spectra are obtained on a Bruker 400/solid-state spectrometer employing magic angle spinning at 12.0 kHz.

RESULTS AND DISCUSSION

1. Compressive Strength

The compressive strength of material is defined as the ability to resist stress without failure. In cementitious materials, compressive strength is of primary importance. In the previous work [11], we found that the weight ratio of fly ash and sodium hydroxide of 12.5 : 1.0 is the proper mixture for alkali-activation of the low-calcium fly ash. Based on the previous experimental analysis, first, in order to verify the proper mixture ratio of fly ash, water glass and sodium hydroxide for the higher strength of paste, some differently mixed activators were employed. The compressive strength of all pastes activated with differently mixed activators is presented in Table 3. Data from Table 3 show that using low-calcium fly ash and activator composed of water glass, sodium hydroxide and water, a high strength paste with compressive strength above 60 MPa can be obtained from paste II and III after curing at 85 °C for 48 hr. Paste IV made from lower content of water glass and paste V made from lower content of sodium hydroxide show lower compressive strength, respectively. Finally, proper activator composition for the higher strength of paste is identified as a weight ratio of water glass, sodium hydroxide and water of 5.25 : 1.0 : 1.25 or 4.0 : 1.0 : 2.5 and activator/fly ash ratio of 0.6.

These results indicate that the water glass and sodium hydroxide content play an important role in the development of compressive strength of the system. Namely, the alkali-activated system required a strongly alkaline solution to promote formation of amorphous aluminosilicate from raw fly ash. The hardening mechanism of the fly ash pastes activated with a water glass solution can be described as follows. The gel-like reaction products from alkali-activated fly ash together with another hydrolysis product (i.e., silical gel) from water glass binds the particles of fly ash and results in the high strength of the pastes. The curing temperature, also, notably affects the development of compressive strength of the pastes. Temperature is a reaction accelerator.

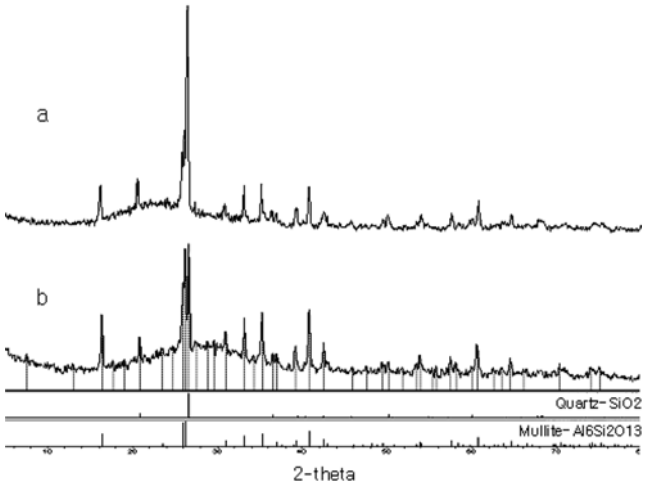

Fig. 1. XRD patterns of unreacted raw fly ash (a) and alkali-activated paste III, (b) at 85 °C for 24 hr with an activator/fly ash ratio of 0.6.

2. XRD Analysis

Fig. 1 shows the XRD patterns for the unreacted raw fly ash and paste III activated at 85 °C for 24 hr with an activator/fly ash ratio of 0.6. In Fig. 1(a), XRD patterns show that the crystalline components of unreacted raw fly ash mainly consist of two major phases, mullite ($3Al_2O_3 \cdot 2SiO_2$) and quartz (SiO_2). In Fig. 1(b), XRD patterns show that alkali-activated fly ash paste also consists of quartz and mullite as the major crystalline phase, which originally exists in the fly ash and has not been changed in the activated paste. These

Table 3. Compressive strength (MPa) of alkali-activated pastes with a activator/fly Ash ratio of 0.6 (wt%)

Paste	Fly ash	Activator (wt %)			Compressive strength (MPa)									
					Curing temperature of 60 °C (times)					Curing temperature of 85 °C (times)				
		Water glass	NaOH	Water	4 hr	6hr	12 hr	24 hr	48 hr	4 hr	6 hr	12 hr	24 hr	48 hr
I	12.5	6.5	1.0	0			16.6	30.7	53.5	26.8	28.3	44.7	48.7	53.2
II	12.5	5.25	1.0	1.25			9.1	35.9	59.9	24.4	26.7	43.4	51.0	63.2
III	12.5	4.0	1.0	2.5	-	-	12.3	25.7	53.0	17.4	26.7	45.0	50.3	60.0
IV	12.5	2.75	1.0	3.75			3.6	11.6	22.0	9.0	5.6	15.0	19.4	30.4
V	12.5	4.0	0.5	3.0			7.2	18.6	34.4	11.3	14.4	24.6	33.7	40.0

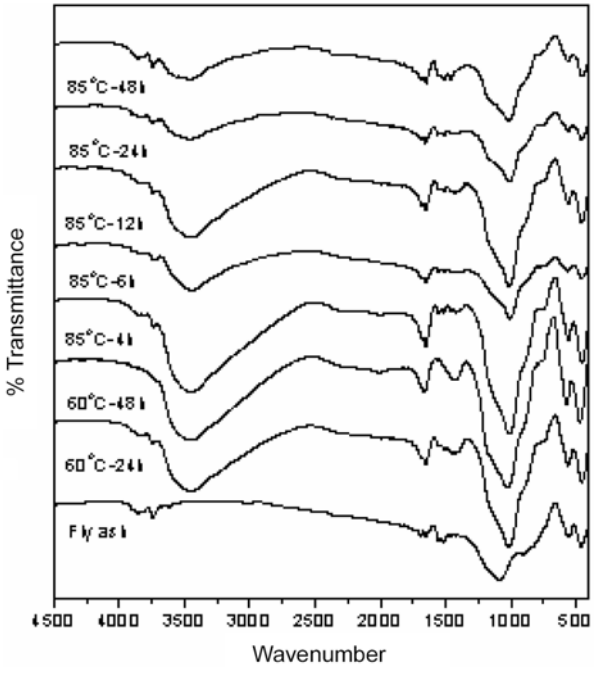

Fig. 2. Infrared spectra of unreacted raw fly ash and alkali-activated paste III at 60 °C and 85 °C for activation times with an activator/fly ash ratio of 0.6, respectively.

results indicate that the main reaction product of alkali-activated fly ash pastes using a water glass solution is "amorphous aluminosilicate gel" with low-order crystalline structure, which does not pattern.

3. FTIR Spectrometer

Fig. 2 shows the FTIR spectra of the unreacted raw fly ash and the alkali-activated fly ash paste III. The spectra of alkali-activated fly ash pastes have a peak at about 3,450 cm^{-1} and 1,650 cm^{-1} due to molecular water (O-H) and deformation (H-O-H), respectively. These bands indicate the presence of some hydration water in the reaction products of alkali-activated fly ash pastes. The FTIR spectra of the alkali-activated fly ash pastes at 60 °C for 24 hr and 48 hr have an absorption peak at 1,425 cm^{-1}. This peak can be ascribed to carbonates in solution, which might be in close association with Na^+ or K^+ cations [12]. Carbonation of alkali-activated fly ash pastes at 85 °C and unreacted raw fly ash disappears or is not observed.

The FTIR spectrum of unreacted raw fly ash shows one main band at about 1,080 cm^{-1}, due to Si-O and Al-O stretching vibrations. In all spectra of the alkali-activated fly ash pastes at 60 °C and 85 °C, for activation times show one main band at about 1,020 cm^{-1} as characteristic bands of "alkaline polymer" corresponding to Si-O and Al-O tension bands. Palomoet al. [10] indicate that this absorption moves towards lower frequencies from the raw fly ash (1,080 cm^{-1}). In all spectra of alkali-activated fly ash pastes and unreacted raw fly ash, a band located at about 456 cm^{-1} is ascribed to (O-Si-O) banding modes of SiO_4 tetrahedra. The alkali-activating reaction hardly affects the band located at 456 cm^{-1} due to (O-Si-O), resulting in almost not shifting the position of the band. Fernández-Jiménez and Palomo [3] published that this band provides an indication of the degree of "amorphization" of the material, since its intensity does not depend on the degree of crystallization. However, the band at about 1,080 cm^{-1} of the unreacted raw fly ash becomes moved towards lower frequencies at about 1,020 cm^{-1} in the activated fly ash, which indicates that the alkaline activation of fly ash leads to the formation of an alkaline aluminosilicate gel of amorphous nature [3]. In all spectra of alkali-activated fly ash pastes and unreacted raw fly ash, another band is observed at about 565 cm^{-1} ascribed to a band present in the starting materials corresponding to mullite.

4. SEM Observation

Fig. 3(a), (b) and (c) show the scanning electron micrographs (×1,000 magnification) of alkali-activated fly ash pastes III at 85 °C for 4 hr, 12 hr and 24 hr with an activator/fly ash ratio of 0.6, respectively. In Fig. 3(a), the matrix of alkali-activated fly ash paste at 85 °C for 4 hr shows the retention of round and smooth spherical fly ash particles, which suggests that some of the raw fly ash has not yet reacted. The unreacting of fly ash is due to the short curing time that is not enough to react with the fly ash. In Fig. 3(b) and (c), the morphology of alkali-activated fly ash pastes at 85 °C for 12 hr and 24 hr shows a more solid and continuous gelatinous matrix due to restructuring of gel-like reaction products from alkali-activated fly ash together with another hydrolysis product (i.e., silical gel) from water glass.

Fig. 4(a), (b) and (c) show the scanning electron micrographs (×10,000 magnification) of alkali-activated fly ash pastes III at 85 °C for 4 hr, 12 hr and 24 hr with an activator/fly ash ratio of 0.6, respectively. Fig. 4(a) shows the formation of an alkaline aluminosilicate gel of amorphous nature from alkaline activation of fly ash together with another hydrolysis product (i.e., silical gel) from water

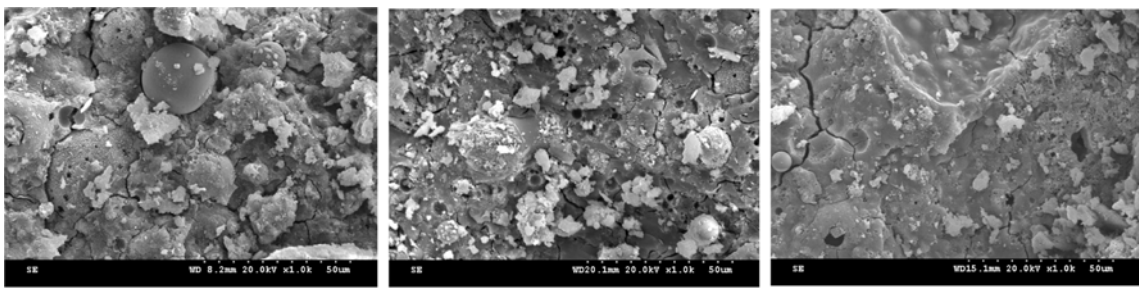

Fig. 3. Scanning electron micrographs (×1,000 magnification) of alkali-activated paste III at 85 °C for 4 hr (a), 12 hr (b), and 24 hr (c) with an activator/fly ash ratio of 0.6, respectively.

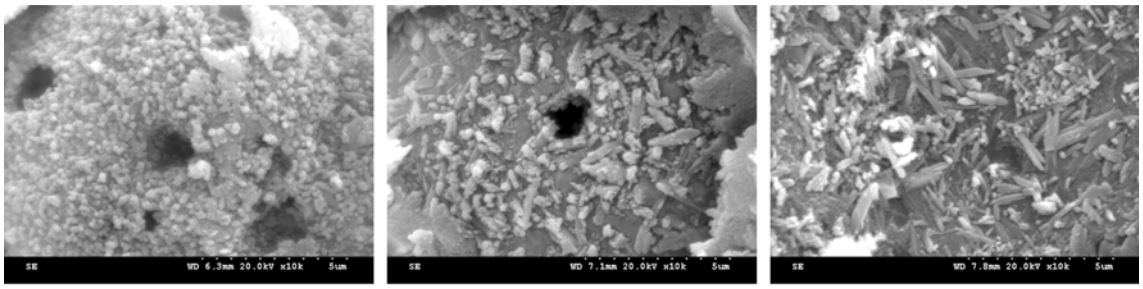

Fig. 4. Scanning electron micrographs (×10,000 magnification) of alkali-activated paste III at 85 °C for 4 hr (a), 12 hr (b), and 24 hr (c) with an activator/fly ash ratio of 0.6, respectively.

glass. This indicates that a large number of the fly ash particles reacted with alkali-activator containing water glass. The fly ash pastes activated for 4 hr and 12 hr show spots of erosion on the spherical surface of the fly ash particles, as can be Fig. 4(a) and (b). The surface erosion of the fly ash particles provides more reactive surface and exposing the mullite crystals, which are originally present in fly ash, resulting in more aluminosilicate solid dissolution. As a result, a series of polysialation, coagulation, colloidal formation, gelation and subsequent gel restructuring take place [8,9] and lead to the high strength of the paste. As shown in Fig. 4(a), (b) and (c), for longer activation times from 4 hr to 12 hr and 24 hr, the amorphous gel is converted into the larger quantity of tabular crystals.

5. Porosity Analysis

The pore-size distribution and accumulated porosity of several pastes are investigated by mercury intrusion porosimetry using a Micromeritics AutoPore IV 9510. For porosity analysis, cylinder specimens of about 0.8 mm diameter and 1 cm height are first degassed under vacuum. The porosities and pore-size distribution of alkali-activated fly ash pastes III at 85 °C for 4 hr, 12 hr and 24 hr with an activator/fly ash ratio of 0.6 are shown in Fig. 5 and Table 4.

As shown in Fig. 5, the paste prepared from alkali-activated fly ash for 4hr, which has the lowest compressive strength in this series of experiments, has highest cumulative pore volume with a diameter

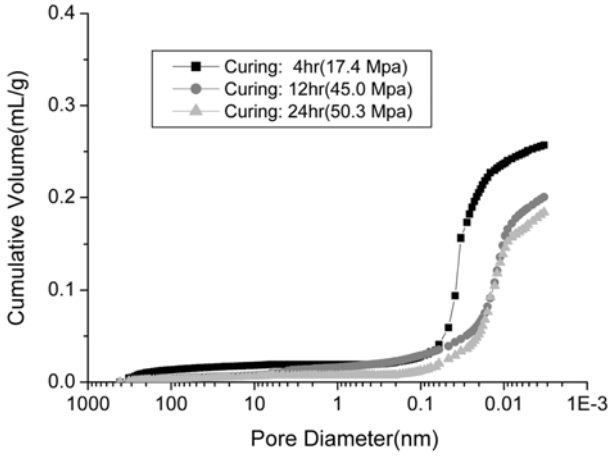

Fig. 5. Pore-size distribution curves of alkali-activated paste III at 85 °C for 4 hr, 12 hr and 24 hr with an activator/fly ash ratio of 0.6, respectively.

ranging from 0.001 to 0.1 nm. In Table 4, the porosities and mean pore diameter of pastes decreased with the prolonged activation time, which indicates a higher densed pore refinement of the microstructure and, consequently, an increase of the compressive strength. The lowest values of both porosity (31.0%) and mean pore diameter (9.7 nm) of the paste from alkali-activated fly ash for 24 hr indicates higher reactivity of this fly ash compared with other pastes, and results in higher compressive strength (50.3 MPa).

6. NMR Analysis

In silicates, solid state ^{29}Si NMR can provide quantitative information on the fraction of silicon present in different tetrahedral environments, Q_n, where n denotes the connectivity of the silicate tetrahedral ($0 \le n \le 4$). Thus Q_o represents isolated tetrahedra, Q_1 denotes chain end group tetrahedral, Q_2 middle groups, Q_3 branching sites, and Q_4 cross-linking sites in a three-dimensional framework [13]. Puertas and Fernández-Jiménez [14] assigned the NMR components according to a basis on values obtained in aluminosilicates as follows. The peaks appearing between −66 and −73 ppm are assigned to Q_o units; between −74 and −78 ppm are assigned to Q_1 units; between −83 and −88 ppm are assigned to Q_2 units; between −95 and −100 ppm are assigned to Q_3 units and between −103 and −115 ppm are assigned to Q_4 units. In aluminosilicates the shifts are further influenced by the replacement of Si by Al in tetrahedra adjacent to a given Si site; generally the substitution of Si by Al shifts a signal 3 or 5 ppm per Al towards more positive values [15].

Fig. 6(a) and (b) show the ^{29}Si solid state NMR spectra of paste III activated at 60 °C and 85 °C for 24 hr with an activator/fly ash ratio of 0.6, respectively, and Fig. 6(c) shows the ^{29}Si solid state NMR spectrum of unreacted raw fly ash. In comparison with the spectrum of unreacted raw fly ash, an important shift of the spectra is detected in alkali-activated fly ash pastes. As shown in Fig. 6(a)

Table 4. Porosities and mean pore diameters of alkali-activated paste III at 85 °C for 4 hr, 12 hr and 24 hr with an activator/fly ash ratio of 0.6, respectively

Items	Paste III		
	4 hr	12 hr	24 hr
Compressive strength (MPa)	17.4	45.0	50.3
Mean pore diameter (nm)	18.5	10.0	9.7
Porosity (%)	38.9	32.6	31.0

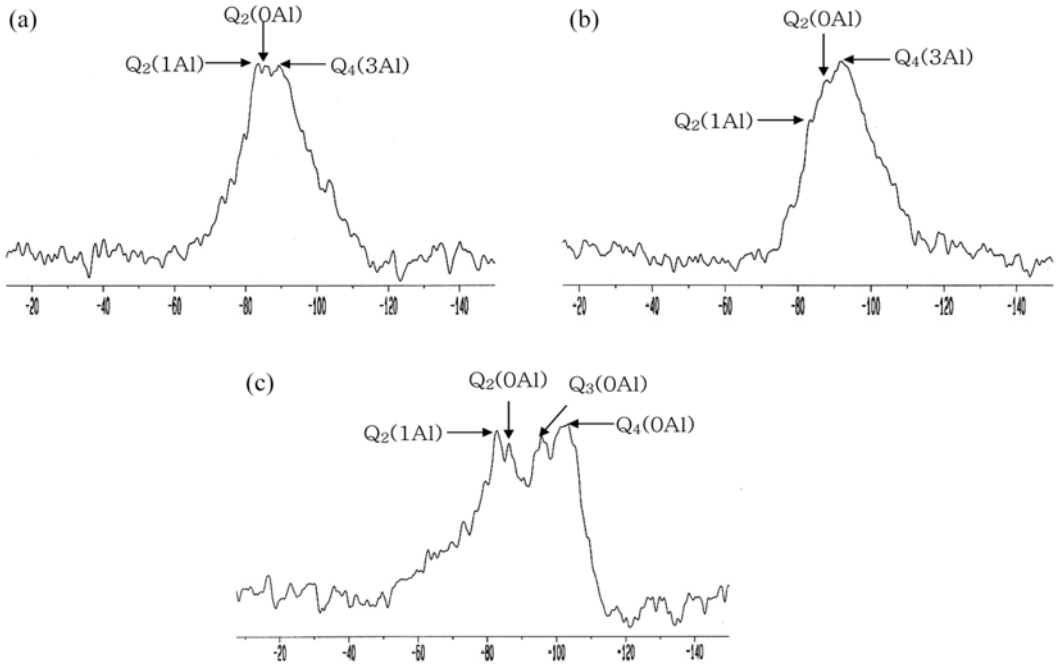

Fig. 6. ^{29}Si solid state NMR spectra of alkali-activated paste III at 60 °C for 24 hr (a) and 85 °C for 24 hr (b) with a activator/fly ash ratio of 0.6, and raw fly ash (c).

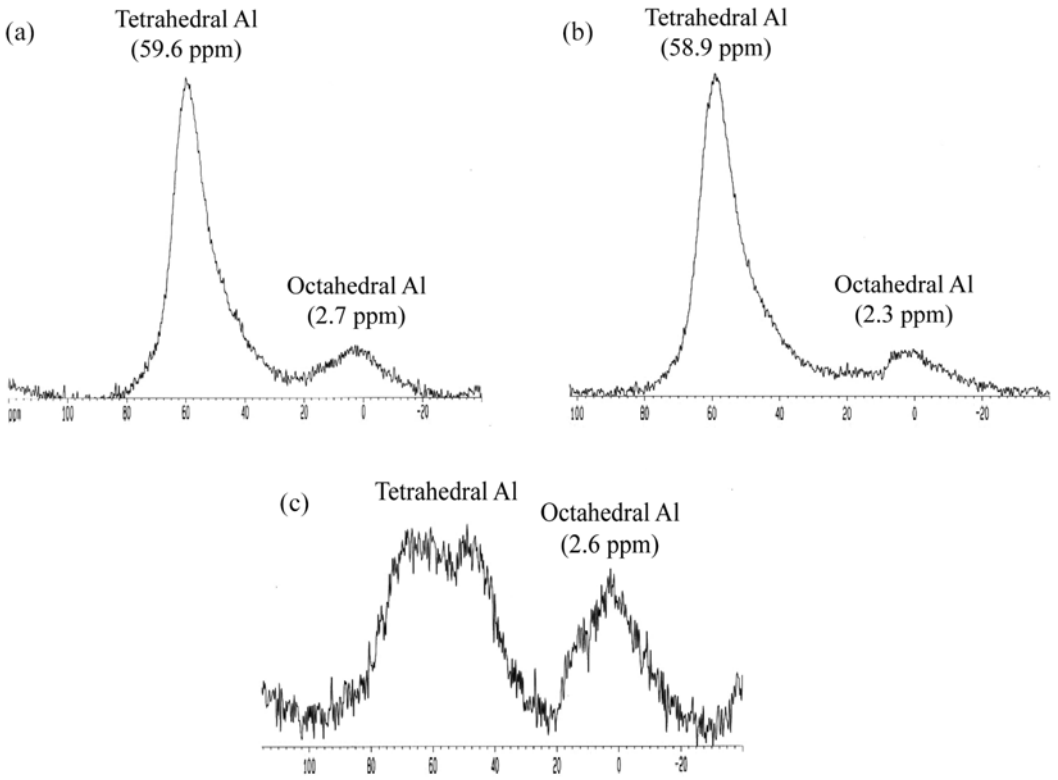

Fig. 7. ^{27}Al NMR solid-state spectra of alkali-activated paste III at 60 °C for 24 hr (a) and 85 °C for 24 hr (b) with a activator/fly ash ratio of 0.6, and raw fly ash (c).

and (b), in alkali-activated fly ash pastes Q_4(3Al) peaks are detected compared to raw fly ash. This peak, Q_4(3Al), indicates the formation of an amorphous alkaline aluminosilicate like a zeolitic gel compound due to the alkaline activation of fly ash [14]. The intensity of the Q_4(3Al) peaks of the paste activated at 85 °C is stronger than that of the paste activated at 60 °C. Also, the Q_4(3Al) peaks seem to be stronger relative to the Q_2 (1Al and 0Al) peaks in paste activated at 85 °C for 24 hr.

^{27}Al NMR solid state spectra can be correlated with defined crystal structures within the inorganic phase [16,17]. Fig. 7(a) and (b) show the ^{27}Al solid state NMR spectra of paste III activated at 60 °C and 85 °C for 24 hr with an activator/fly ash ratio of 0.6, respectively, and Fig. 7(c) shows the ^{27}Al solid-state NMR spectrum of unreacted raw fly ash. ^{27}Al solid state NMR spectra of alkali-activated fly ash pastes at 60 °C and 85 °C for 24 hr have tetrahedral aluminum and octahedral aluminum, but the relative quantity of tetrahedral aluminum is larger in this case as shown in Fig. 7(a) and (b). The octahedral peaks are significantly broader asymmetric signal centered at +2.7 ppm (Fig. 7(a)) and +2.3 ppm (Fig. 7(b)). It is apparent that most of the aluminum in the alkali-activated fly ash pastes is tetrahedrally coordinated. The tetrahedral aluminum in the alkali-activated fly ash pastes explains the presence of the Al in the alkaline aluminosilicate hydrated with a three-dimensional structure. In Fig. 7(c), unreacted raw fly ash shows the broad tetrahedral aluminum and octahedral aluminum, corresponding to the lower degree of crystallinity. Octahedral aluminum (+2.6 ppm) of unreacted raw fly ash can be interpreted as assigned to that of mullite.

CONCLUSIONS

Water glass and sodium hydroxide content play an important role in the development of the compressive strength of the alkali-activated fly ash pastes. The morphology of alkali-activated fly ash pastes shows a more solid and continuous gelatinous matrix due to restructuring of gel-like reaction products from alkali-activated fly ash together with another hydrolysis product (i.e., silical gel) from water glass. The porosities and mean pore diameter of pastes decreased with the prolonged activation time, which indicates the higher densed pore refinement of the microstructure, and results in higher compressive strength. The intensity of Q_4(3Al) peaks of the paste activated at 85 °C is stronger than that of the paste activated at 60 °C, which this peak indicates the formation of an amorphous alkaline aluminosilicate in alkali-activated fly ash pastes. Also, most of the aluminum in these pastes is tetrahedrally coordinated.

ACKNOWLEDGMENT

This work was supported by grant No. R01-2004-000-10480-0 from the Basic Research Program of the Korea Science & Engineering Foundation.

REFERENCES

1. D. Li, Z. Xu, Z. Luo, Z. Pan and L. Cheng, *Cement & Concrete Composites*, **32**, 1145 (2002).
2. A. Guerrero, S. Goñi, A. Macías and M. P. Luxán, *J. Mater. Res.*, **14**, 2680 (1999).
3. A. Fernández-Jiménez and A. Palomo, *Cement & Concrete Research*, **35**, 1984 (2005).
4. X. Zhaohui and X. Yunping, *Cement & Concrete Research*, **31**, 1245 (2001).
5. R. Hossein and B. William, *Environ. Sci. Technol.*, **37**, 3454 (2003).
6. A. Samdi, PhD dissertation of Drexel University, *Treatment of fly ash to increase its cementitious characteristics*, Philadelphia, PA (1996).
7. P. Arjunan, M. R. Silsbee and D. M. Roy, *Chemical activation of low calcium fly ash: Part: Identification of the most appropriate activators and their dosage*, Proceedings of the Intl. Ash Utilization Symposium, Kentucky (2001).
8. Van J. G. S. Jaarsveld and Van J. S. J. Deventer, *Miner. Eng.*, **10**, 659 (1997).
9. J. Davidovits, *J. Mater. Eng.*, **16**, 91 (1994).
10. A. Palomo, M. W. Grutzeck and M. T. Blanco, *Cement & Concrete Research*, **29**, 1323 (1999).
11. S. S. Park and H. Y. Kang, *Korean J. Chem. Eng.*, **23**, 367 (2005).
12. V. F. F. Barbosa, K. J. D. MacKenzie and C. Thaumaturgo, *Int. J. Inorg. Mater.*, **2**, 309 (2000).
13. I. G. Richardson, A. R. Brough, G. W. Groves and C. M. Dobson, *Cement & Concrete Research*, **24**, 813 (1994).
14. F. Puertas and A. Fernández-Jiménez, *Cement & Concrete Composites*, **25**, 287 (2003).
15. G. Engelhardt and D. Michel, *High resolution solid state NMR of silicates and zeolites*, Wiley (1987).
16. J. Skibsted, E. Henderson and H. J. Jakobsen, *Inorg. Chem.*, **32**, 1013 (1993).
17. M. D. Andersen, H. J. Jakobsen and J. Skibsted, *Inorg. Chem.*, **42**, 2280 (2003).
18. A. Palomo and J. I. López de la Fuente, *Cement & Concrete Research*, **33**, 281 (2003).